Pterodactyl: Thermal Protection System for Integrated Control Design of a Mechanically Deployed Entry Vehicle

Zane B. Hays*
STC, Inc., Moffett Field, CA, 94035 Research Assistant, STC, Inc.

Bryan C. Yount §, Ben E. Nikaido ‡, Jason Tran ¶, Sarah N. D'Souza**, David J. Kinney ***, and M. Kathleen McGuire ††
NASA Ames Research Center, Moffett Field, CA, 94035

The need for precision landing of high mass payloads on Mars and the return of sensitive samples from other planetary bodies to specific locations on Earth is driving the development of an innovative NASA technology referred to as the Deployable Entry Vehicle (DEV). A DEV has the potential to deliver an equivalent science payload with a stowed diameter 3 to 4 times smaller than a traditional rigid capsule configuration. However, the DEV design does not easily lend itself to traditional methods of directional control. The NASA Space Technology Mission Directorate (STMD)'s Pterodactyl project is currently investigating the effectiveness of three different Guidance and Control (G&C) systems – actuated flaps, Center of Gravity (CG) or mass movement, and Reaction Control System (RCS) – for use with a DEV using the Adaptable, Deployable, Entry, and Placement Technology (ADEPT) design. This paper details the Thermal Protection System (TPS) design and associated mass estimation efforts for each of the G&C systems. TPS is needed for the nose cap of the DEV and the flaps of the actuated flap control system. The development of a TPS selection, sizing, and mass estimation method designed to deal with the varying requirements for the G&C options throughout the trajectory is presented. The paper discusses the methods used to i) obtain heating environments throughout the trajectory with respect to the chosen control system and resulting geometry; ii) determine a suitable TPS material; iii) produce TPS thickness estimations; and, iv) determine the final TPS mass estimation based on TPS thickness, vehicle control system, vehicle structure, and vehicle payload.

* Junior Research Analyst, Systems Analysis Office, NASA ARC/AA.
§ Experimental Facility Developer, Engineering Systems Division, NASA ARC/RE.
‡ Aerospace Flight System Engineer, Systems Analysis Office, NASA ARC/AA.
¶ Graduate Pathways Student, Systems Analysis Office, NASA ARC/AA.
** Principal Investigator, Systems Analysis Office, NASA ARC/AA.
*** Flight System Engineer, Systems Analysis Office, NASA ARC/AA.
†† Aerospace Flight Systems, Systems Analysis Office, NASA ARC/AA.

I. Nomenclature

α	=	Angle of Attack (Alpha)
ADEPT	=	Adaptable, Deployable Entry Placement Technology
β	=	Sideslip Angle (Beta)
DEV	=	Deployable Entry Vehicle
G&C	=	Guidance and Controls
HEEET	=	Heatshield for Extreme Entry Environment Technology
OML	=	Outer Mold Line
PBV	=	Pterodactyl Baseline Vehicle
RCS	=	Reaction Control System
TPS	=	Thermal Protection System

II. Introduction

Thermal Protection Systems (TPS) are essential components for atmospheric entry vehicles and often impact mission capabilities significantly. As new technologies and methods for entry are developed, the processes used to determine TPS thicknesses must also adapt to new challenges. The Pterodactyl project at NASA Ames Research Center (Ref. [1]) pushes TPS analysis methods into a more complicated realm than that of the common bank control and ballistic entry vehicle problem. The complication arises from the non-traditional vehicle configuration being considered by the Pterodactyl group for precision targeting. Specifically, the Pterodactyl group is investigating novel control systems for integration with a Deployable Entry Vehicle (DEV) as discussed in Ref [2]. The current state-of-the-art for precision targeting of traditional entry vehicles is rooted in rigid entry vehicles such as Mars Science Laboratory and Apollo, which primarily utilize reaction control system (RCS) thrusters attached to the back shell to control the bank angle of the vehicle (Ref. [3]). In contrast, the Pterodactyl Baseline Vehicle (PBV) (Ref. [2]), a modified DEV-style vehicle, has no back shell on which to attach a G&C system. In addition, the Pterodactyl group was investigating novel control effectors which could provide sufficient control authority to meet precision targeting requirements (Ref. [1]). The Pterodactyl group's primary focus was on three different control effectors: i) flap control system, ii) mass movement control system, and iii) RCS.

The TPS analyses for mass movement and RCS align with traditional approaches for TPS sizing because neither of these control effectors are exposed to the high heat flow field. However, for the flap control system, control surfaces are dynamically exposed to the high heat flow field and therefore require a TPS. Current TPS sizing and analysis tools allow for a single static geometry for a given trajectory and are not set up to handle the flap control system's morphing geometry. Therefore, adaptations to current tools were developed and implemented to enable analysis of the changing geometry caused by varying flap deflections throughout the trajectory. In addition, these adaptations account for varying sideslip angles which allow for more complicated angle of attack-sideslip angle trajectories to be explored. In the following sections a flap control surface TPS sizing method, including capabilities for both sideslip angle trajectories and shape morphing geometries, is described.

III. Method Overview

The main intent of this analysis method is to extend the capabilities of TPSSizer (Ref. [4]) and CBAERO (Ref. [5]) to encompass morphing geometries and sideslip angles in order to perform an accurate TPS sizing analysis of the PBV. The following steps were used to perform the TPS analysis: acquire inputs, select TPS material, determine the geometry changes required, run CBAERO for each sideslip angle at each geometry change, run CBTPS on each CBAERO database, interpolate the CBTPS results to match the required control commands and trajectory parameters, apply bump factors to the heating environments, and run TPSSizer on the resulting bumped CBTPS database. Fig. 1 shows a flow diagram of the analysis.

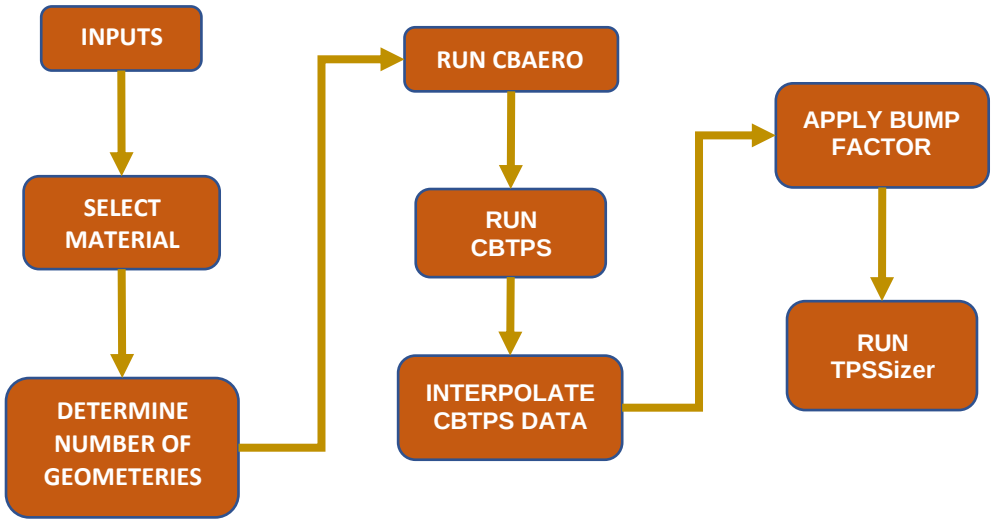

Fig. 1: Analysis Flow Diagram

A. Assumptions

Several assumptions were made to reduce the complexity of the TPS sizing analysis presented in this paper. It was assumed that the PBV's aft body's TPS design would not greatly impact the vehicle mass and thus could be excluded from the analysis. As the RCS jets were angled back away from the vehicle's payload and skirt, the fluid interactions with the aft body were also assumed to cause little effect on the TPS mass and were neglected from the analysis. The sizing of the PBV's carbon fabric skirt was assumed to be out of scope for this analysis and was sized using a rule of thumb that relates maximum heat rate to the number of carbon fabric layers as discussed in Ref. [2]. The nose cap for all three G&C methods experience similar heating through their respective trajectories (Ref. [6]), so it was assumed that the nose cap could be sized for all cases using the flap method's G&C trajectory. The aerodynamics group assumed that for the G&C flap method, the flaps' flow interactions were decoupled from each other as discussed in Ref. [7]. Using on this assumption, the TPS group was able to analyze individual flap heating and did not have to account for interactions between adjacent flaps. Finally, it was assumed that a one-dimensional, engineering-level TPS analysis would be sufficient for the purposes of this trade study.

B. Vehicle Geometry

The PBV is a DEV designed to deliver a relatively large payload for the allowable stowed diameter of a launch vehicle in comparison to a more traditional rigid vehicle. The lifting nature of the vehicle provides for an increased cross range, permitting a wide range of landing options. The PBV is comprised of three sections, as shown in Fig. 2a.

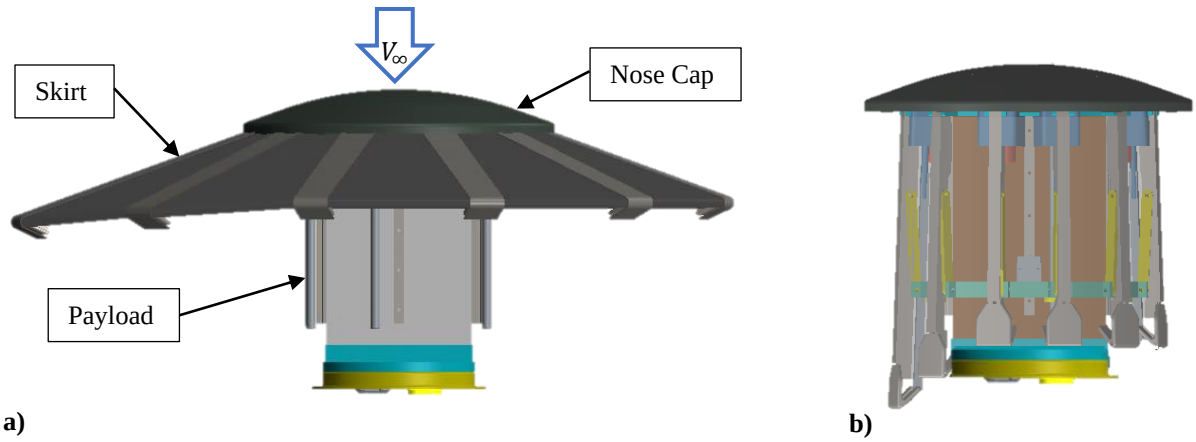

Fig. 2: PBV without G&C modifications

The skirt section is folded up around the central payload on launch, shown in Fig. 2b, and is deployed on entry to act as an extension of the heat shield, shown in Fig. 2a. The nose cap is designed to take the peak entry heating by using a solid, more traditional TPS. The geometry remains constant for all three G&C methods being investigated. Only the actuated flap method adds components that interact with the external flow field around the vehicle, causing it to require further TPS analysis. Fig. 3a shows the flap geometry attached to the PBV and Fig. 3b demonstrates the definition of positive and negative flap deflection angles. The hinge point, located such that the hinge rotates smoothly around the rib tip radius, allows for flap deflection angles between -45° and 20°.

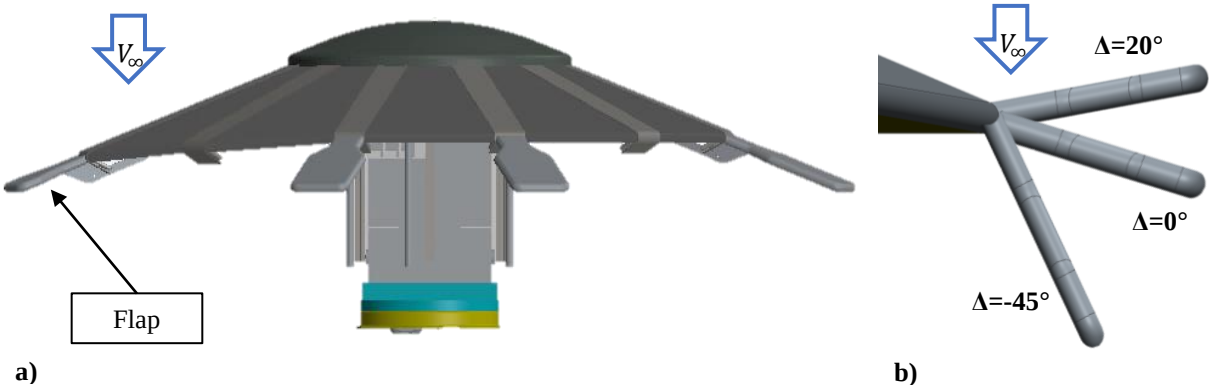

Fig. 3: PBV flap G&C configuration

As each flap's heating environment was assumed to have no impact on the two adjacent flaps, there was no need to create geometries for all possible combination of flap deflections. Instead, five geometries were created with all flaps at the following deflection angles: -45°, -20°, 0°, 10°, & 20°. Fig. 4 shows the flow facing geometry for all eight flaps at 0° deflection.

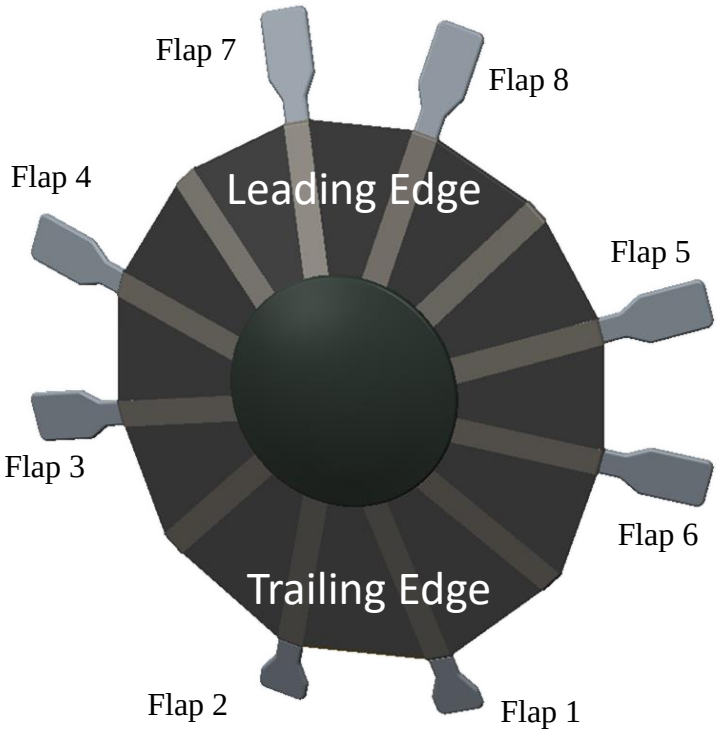

Fig. 4: PBV with Integrated Flaps at 0° Deflection

To account for the combinations of flaps seen at any point in the trajectory, each flap's deflection angle was derived by interpolating between the nearest of the five geometries run. Thus, at a given point in time, each of the eight flaps may be deflected at a unique angle to match the required entry control schema.

C. Aerodynamics, Controls, and Trajectory

The PBV was flown through a lifting lunar return trajectory detailed in Ref. [6]. As mentioned above, the flap G&C trajectory was used to size both the nose cap and flap TPS. The aerodynamics group decided to create a large solution space surrounding all likely trajectories because the trajectory was being iterated for control methods and geometry changes. The aerodynamic parameter bounds used for the trajectory solution space are discussed in depth in Ref. [7] and summarized in Table 1 below.

Table 1: Aerodynamic Parameter Bounds

Parameter	Maximum	Minimum
Angle of Attack	0°	-20°
Sideslip Angle	10°	-10°
Mach Number	40.1	2
Dynamic Pressure	3090 Pa	1.2 Pa

The aerodynamics group selected a set of values across the solution space, including the bounding values, to form the aerodynamic run matrix. Once the trajectory converged to the final solution, a controls schema for the flaps was determined as discussed in Ref. [8] and shown in Fig. 5.

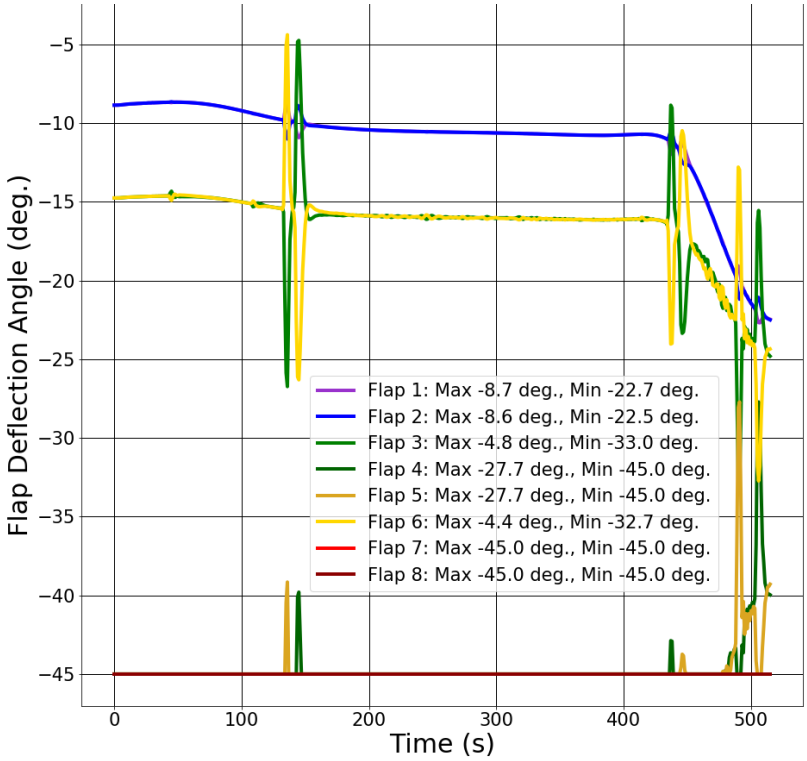

Fig. 5: Flap deflection angles through trajectory

D. Required Inputs

The TPS analysis requires input geometries, a high-fidelity aerodynamic database, a controls schema, and a trajectory. A list of the required input parameters is shown in Fig. 6 below.

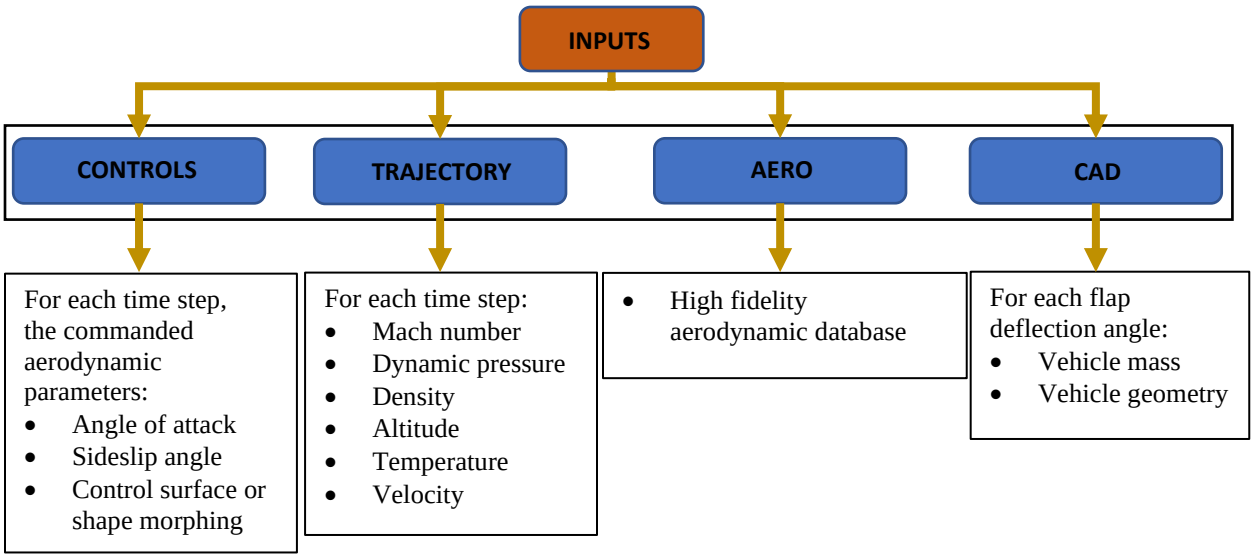

Fig. 6: Required input data

The uncertainty of the aero-thermodynamic environments produced from CBAERO can be reduced by anchoring the CBAERO data to high-fidelity aerodynamic data at several points. The number of high-fidelity points needed for an accurate TPS analysis depends on the complexity of the geometry and the trajectory flown. For example, a capsule entry vehicle is a relatively simple geometry and could be modeled accurately with as few as four high-fidelity points. However, if the vehicle is more complicated and has flaps that actuate in and out of the flow field, it is essential to define several of these flap positions with high-fidelity points in order to accurately capture performance.

E. Tools

A combination of several engineering-level analysis tools was employed to perform the TPS analysis. CBAERO (Ref. [5]) predicts the aerodynamic and aero-thermodynamic environments for a given vehicle. The predictions are calculated for a single geometry with a single sideslip angle for a list of Mach numbers, dynamic pressures, and angles of attack and saved in a database. The CBAERO distribution has a utility, CBTPS, which uses the environments database and a trajectory to calculate the aero-thermodynamic environment time history required for TPSSizer. TPSSizer (Ref. [4]) is a tool designed to work with CBAERO and FIAT (Ref. [9]) to determine the required TPS thickness for specified sizing points on a vehicle flown through a given trajectory. TPSSizer calculates the mass and optimizes TPS thickness for both non-ablative and ablative TPS materials, while satisfying the allowable temperature constraints applied to the TPS material stack-up. These tools were wrapped in a Python script to extend their capabilities to multiple sideslip angles and morphing geometries.

F. TPS Analysis Methodology

The analysis method aims to extend the capabilities of TPSSizer and CBAERO to encompass varying geometries and sideslip angles. The first step is to obtain the required inputs to run CBAERO and TPSSizer. Next, the TPS material is selected. For the Pterodactyl project, several alternatives for the material were examined for the nose cap. The material that minimized the step between nose cap and skirt was chosen to be the final nose cap TPS material. The flaps' TPS material was chosen based on structural strength and TPS thickness. Once the material was chosen, CBAERO and CBTPS were run for each sideslip angle and geometry change. In the case of the Pterodactyl's flap control system, 25 databases were created, one for each of the five sideslip angles (-10°, -5°, 0°, 5°, & 10°) at each of the 5 flap deflection angles (-45°, -20°, 0°, 10°, & 20°). As explained above, the 5 flap deflection angle geometries were constructed using the PBV with the all 8 flaps rotated to the same deflection angle. Nine databases where constructed, one for each of the 8 flaps and one for the nose cap. These databases contained the respective aero-aeroheating dynamic environments pulled from the 25 CBTPS flap runs and the 5 CBTPS nose cap runs (one for each sideslip angle). Next, the databases were interpolated to match the control scheme at each time step in the trajectory, creating 9 new aero-aerothermal dynamic environments, one for each of the 8 flaps and one for the nose cap.

For the simple geometry of the nose cap, CBAERO captured the heating well enough and a bump factor was not needed. The flaps, however, have a much more complicated geometry, and needed higher fidelity CFD to capture the more complicated flow. A bump factor was created using high-fidelity aerodynamics from Cart3D (Ref. [10]) with

real gas effects and applied to the flap databases. The bump factor was applied via the film coefficient because FIAT uses film coefficient and recovery enthalpy to calculate heating. The bump factor applied to the film coefficient was based on the heat rate at a stagnation point using Tauber's equation and is discussed in Ref. [11]. The evaluation of the velocity gradient at a hemispherical stagnation point using Newtonian theory provides a relationship between velocity gradient and the square root of the ratio of freestream pressure and stagnation pressure. As the film coefficient is a function of the edge velocity (Ref. [12]), a reasonable relationship between convective heating and pressure can be established. The resulting relationship between the enthalpy-based film coefficient and the pressure ratio of the high-fidelity pressure to CBAERO pressure results is a better estimate of the more complicated aerodynamic shock and pressure interactions around the flap geometry. Equation (1) shows the form of the bump factor used in this analysis.

$$Bump\ \ Factor\ (BF) = \sqrt{\frac{Pressure_{High\ fidelity}}{Pressure_{CBAero}}} \tag{1}$$

The bump factor was bounded so it would be greater than or equal to 1.0. It is then applied to the CBAERO film coefficient, as Eq. (2) illustrates.

$$C_{film\ final} = C_{film\ CBAero} \cdot (BF) \tag{2}$$

This approximation helps to account for some of the shock-shock interactions observed around the flaps. Once the bump factor was applied to the film coefficient at each time step in the trajectory, the aero-aerothermal dynamic environments were re-built using the new film coefficients. These eight bumped, aero-aerothermal dynamic environments and the nose cap aero-aerothermal dynamic environments were input into TPSSizer, which used FIAT to determine the resulting masses and optimized TPS thicknesses for each of the nine regions of interest.

IV. Nose Cap Analysis and Results

A single CAD model and the flap configuration G&C trajectory and controls schema with the appropriate input parameters were provided for the nose cap TPS sizing analysis.

A. Nose Cap Geometry, Aerothermal, and TPS Selection and Analysis

The nose cap of the asymmetric, ~1-meter diameter PBV's nose cap is shown in red in Fig. 7. The shape change due to recession for the nose cap TPS was predicted to be minimal, so a single geometry Outer Mold Line (OML) was used. However, due to the five different sideslip angles required for the trajectory solution space and control scheme, the single OML was run five times in CBAERO to cover the aerodynamic solution space.

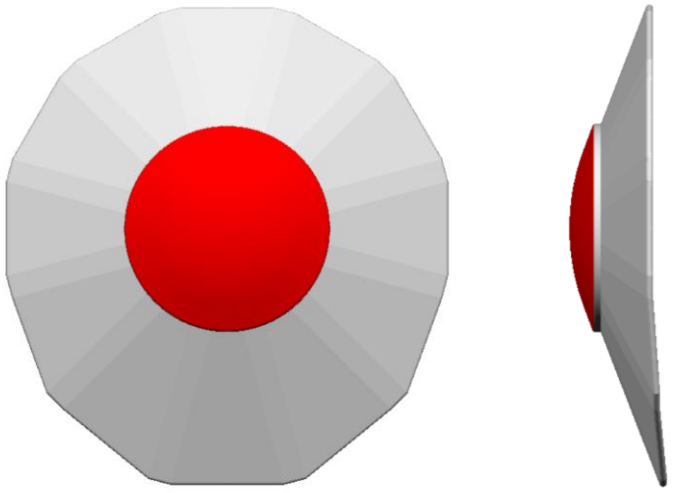

Fig. 7: PBV Nose Cap Geometry

Based on the CBAERO results, expert opinion, and group interest, three TPS materials for the nose cap were examined: PICA (Ref [13]), C-PICA (Ref [14]), and 2D Carbon phenolic (Ref [15]). TPS aerothermal sizing analyses were run for each option to determine approximate trends between the different materials. Fig. 8 illustrates the material stack-ups for the three different TPS options.

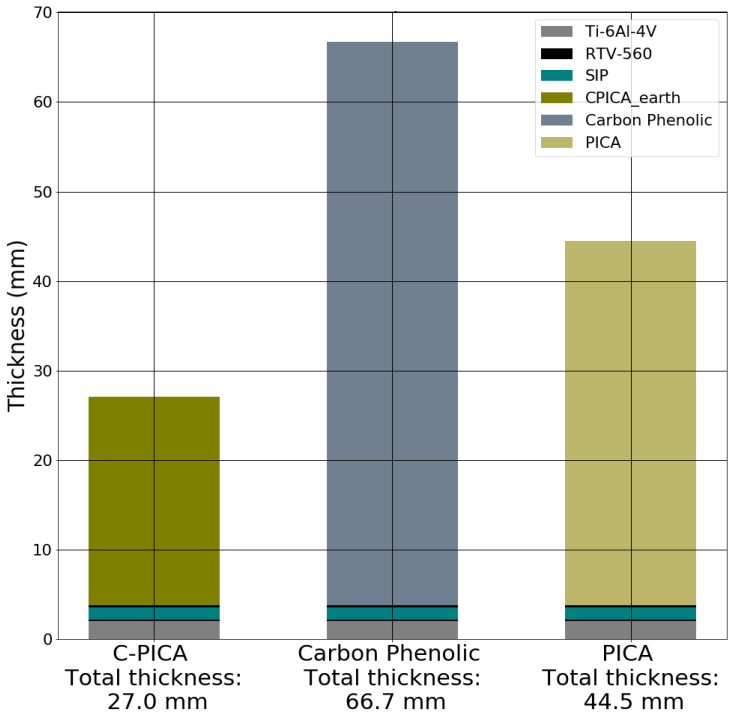

Fig. 8: Nose Cap TPS Stack-ups

As discussed earlier, the nose cap TPS material selection was based on TPS thickness. The analysis indicated that the use of C-PICA resulted in the thinnest material stack, so it was chosen for the nose cap throughout the rest of the analysis cycle.

B. Nose Cap Analysis

The CBTPS aero-aerothermal dynamic environment files were interpolated to match the trajectory's sideslip angle conditions and TPSSizer was run. The resulting nose cap heat rate versus time for this trajectory is shown in Fig. 9.

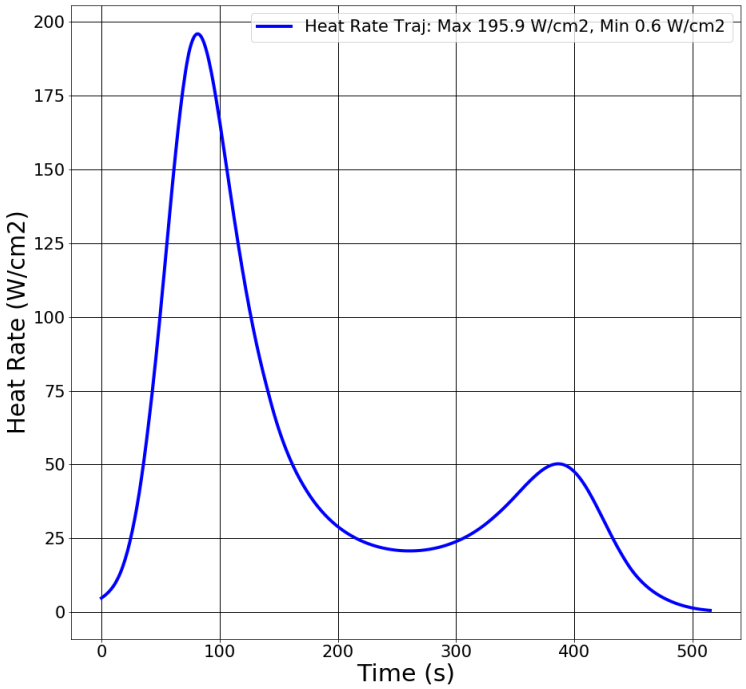

Fig. 9: Nose Cap Heat Rate vs. Time

Next, it was noted that C-PICA's ablation should be negligible when the amount of dissociated oxygen is small. Fig. 10, which shows a time history of the amount of dissociated oxygen for the trajectory, was consulted to determine when the amount of dissociated oxygen was below $10^{-5}\frac{kg}{kmol}$. The ablation was turned off after this point in the trajectory (433 seconds) so that the recession and final TPS thickness would not be over-predicted.

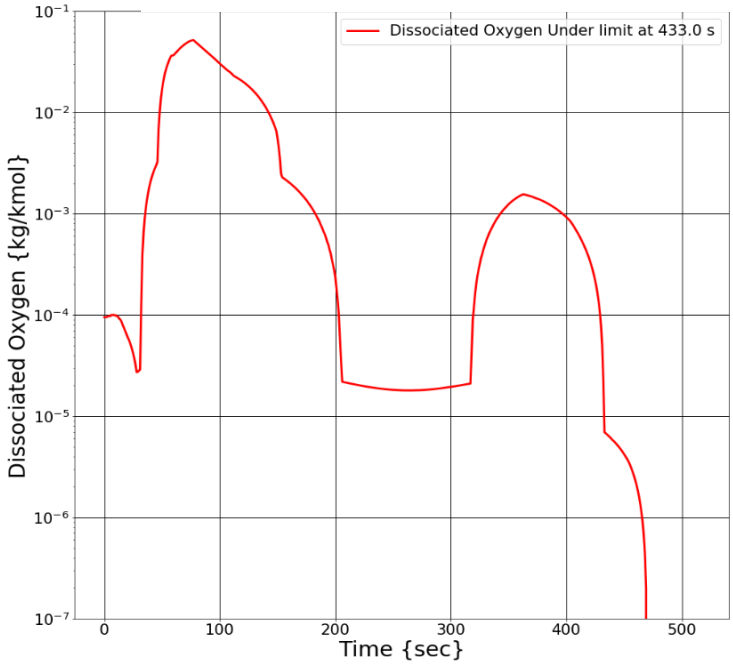

Fig. 10: C-PICA Dissociated Oxygen vs. Time

C. Nose Cap Results

The sizing analysis predicted that the PBV's nose cap requires a C-PICA thickness of 27.0 mm (1.06 inches) resulting in a mass of 1.22 kg (2.68 lb). The total amount predicted of recession was 8.0 mm, measured from the OML. The final material stack-up is shown below in Fig. 11.

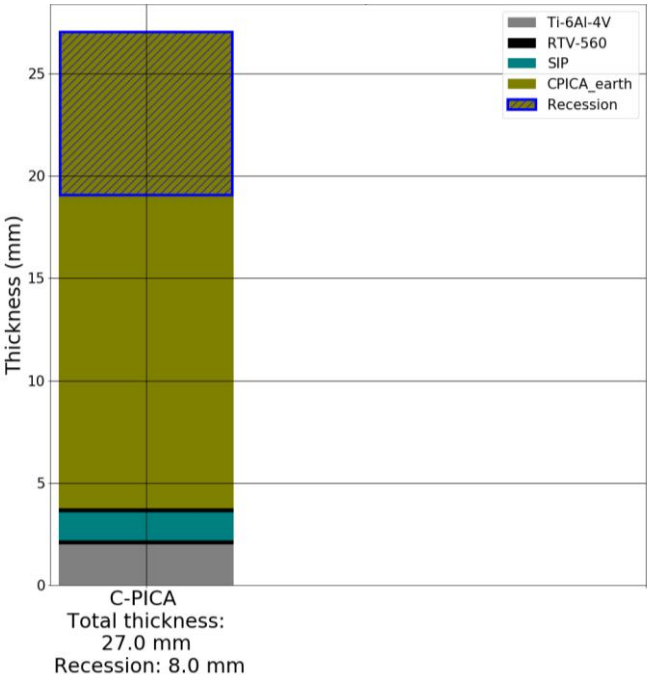

Fig. 11: C-PICA Nose Cap Material Stack-up Thicknesses

V. Flap Analysis and Results

There are two main differences between the nose cap analysis and the flap analysis – the number of required geometries and the complexity of those geometries. Due to the complex nature of the flow around the flap geometry resulting from deflections, the CBAERO anchoring process was used to increase the accuracy of the aerodynamic and aeroheating predictions by incorporating high-fidelity aerodynamics. Cart3D was chosen to be the high-fidelity CFD code used by the aerodynamics group (Ref. [7]) to compute the anchoring cases. The flap analysis was performed using the same PBV geometry and trajectory inputs used for the nose cap, with the addition of the flap control data and flap geometries.

A. Flap TPS Material Selection

To ensure an adequate seal between the flap and the PBV's rib tip, the mechanical design group requested the thinnest flap possible to aid with integrating the flaps onto the PBV. To accomplish this, much of the flap structure had to be made of TPS material, resulting in the need for a TPS material option that could act as a structural component. Two materials were initially considered - 2D carbon phenolic (Ref [15]) and Heatshield for Extreme Entry Environment Technology (HEEET) (Ref [16]) because they both can sustain structural loads. However, 2D carbon phenolic, while strong, is brittle and highly conductive (Ref [15]). As the flaps would be placed under varying aerodynamic loads during the trajectory, the brittle nature of 2D carbon phenolic was deemed structurally inadequate. Additionally, carbon phenolic is highly conductive and would result in a large amount of heat flowing directly to the hinge joint, requiring a thicker layer of TPS to maintain the joints structural integrity. The alternative, HEEET, was developed to meet needs for extreme heating entry environments and is comprised of 3D woven layers of carbon fabric injected with medium density phenolic resin to create a dense solid which was tested to withstand 6000 $\frac{W}{cm^2}$ (Ref. [16]). HEEET consists of two layers. The outer recessive layer is comprised of high density all carbon layers and the inner insulative layer is made from a combination of lower density carbon and phenolic yarns (Ref. [16]). The dual layers allow for structural integrity while maintaining a lower thermal conductivity than carbon phenolic. To verify HEEET could meet the structural strength needed for the Pterodactyl's trajectory, an FEA model was

constructed to determine that the flap can sustain the maximum forward-facing pressure load of 8230 Pa, the maximum seen during the trajectory. Fig. 12 shows the FEA model with the von Mises Stress on the Titanium spar due to the pressure load. The stress and deflection values were determined to be well below the allowable limits for the material. Therefore, HEEET was chosen over carbon phenolic for its superior thermally and structurally properties when applied to the PBV's flap application.

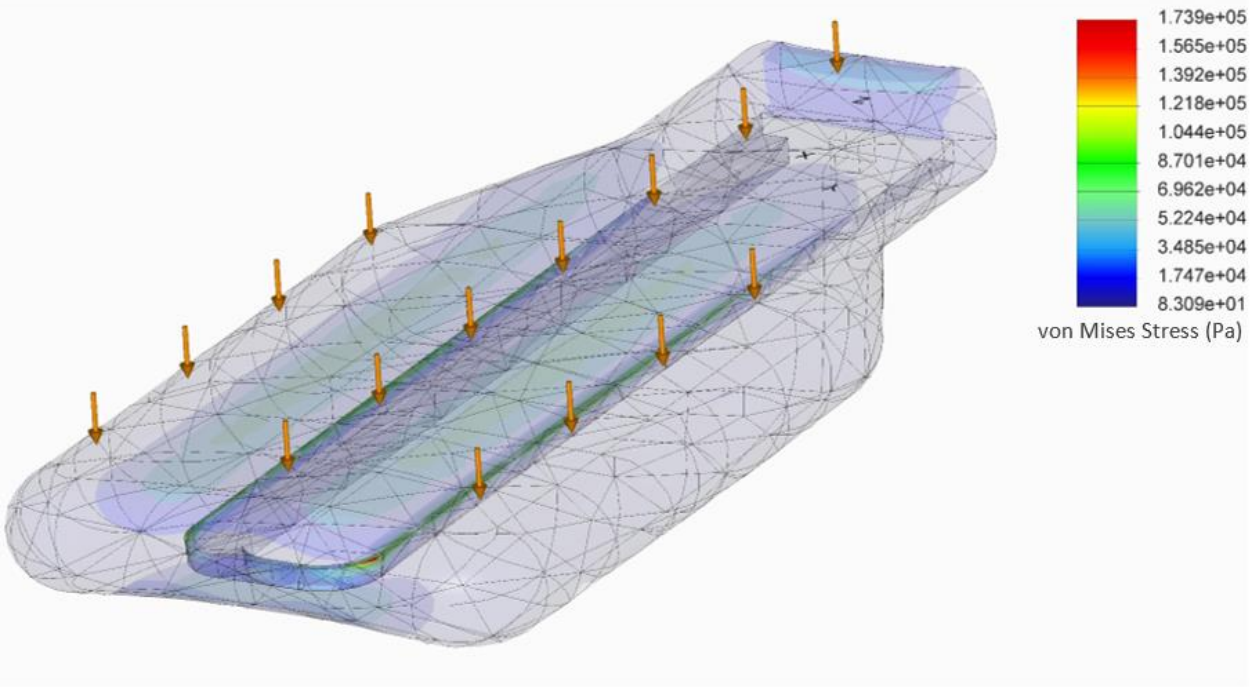

Fig. 12: HEEET Maximum Forward-facing Pressure load FEA Model

TPS thickness optimization is typically driven by the material layer in the stack-up with the lowest allowable maximum temperature. In many cases this is the adhesive used to attach the TPS to the structure. To further reduce the required TPS thickness for this problem, the TPS flap structure was designed with a mechanical rather than adhesive attachment, greatly increasing the design's maximum allowable internal temperature constraint. The design uses a titanium spar pinned inside of a HEEET sleeve, as shown in Fig. 13. This results in a material stack-up from bottom to top consisting of titanium, HEEET insulative layer, and HEEET recessive layer.

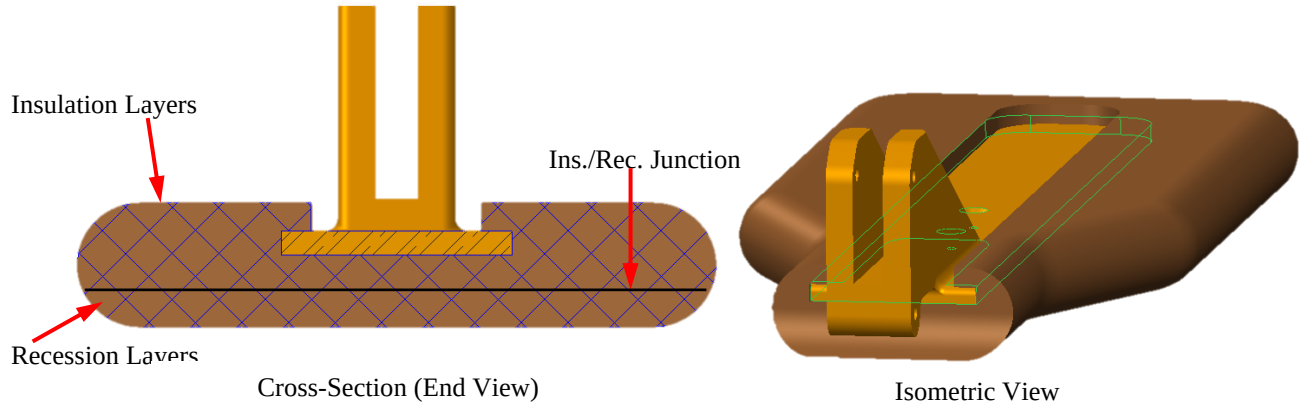

Fig. 13: HEEET Flap Design

Each flap encounters slightly different heating environments. Rather than sizing each flap independently, it was decided to choose the point that experienced the worst integrated heating to size all the flaps. The thermal response of the flap design is highly multi-dimensional due to the relatively small size of the flap, the small radii on the flap edges, the various angles of the flap relative to the flow, and the high in-plane thermal conductivity of HEEET and titanium. However, the analysis tools being used, TPSSizer and FIAT, perform 1D thermal optimization at discrete

point locations. This makes it difficult to determine ahead of time which location on the flap will result in the thickest optimized TPS. To get around this limitation, several points on the surface were used as sizing points throughout the analysis, as shown in Fig. 14. Fig. 14 shows the pressure distribution over the flap and the eight sizing points chosen for this analysis. A total of 64 analysis points, eight points per flap, were run through the aerothermal dynamic analysis and the point with the largest integrated heat load was used to size the final flap TPS.

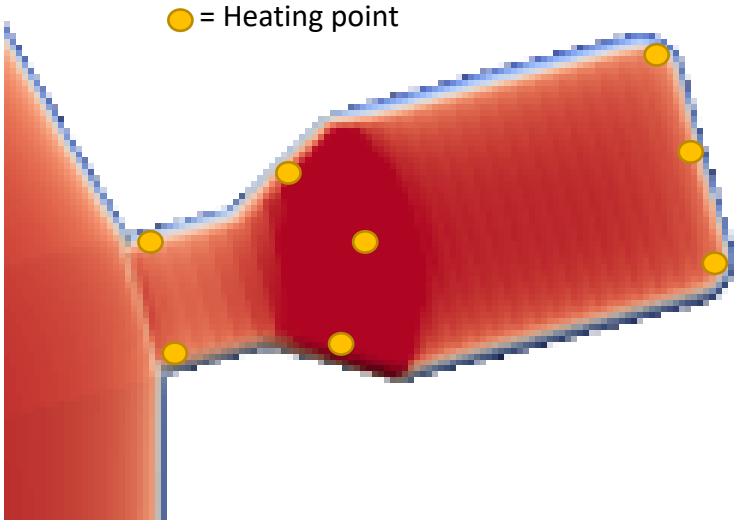

Fig. 14: Flap Heating Points

B. Flap Bump Factor and Aeroheating

The bump factors were calculated for each flap at each deflection angle using the ratio of the Cart3D to the CBAERO pressure data. Flap #3's deflection angle, Cart3D pressure, CBAERO pressure, and bump factor applied film coefficient are shown in Fig. 15.

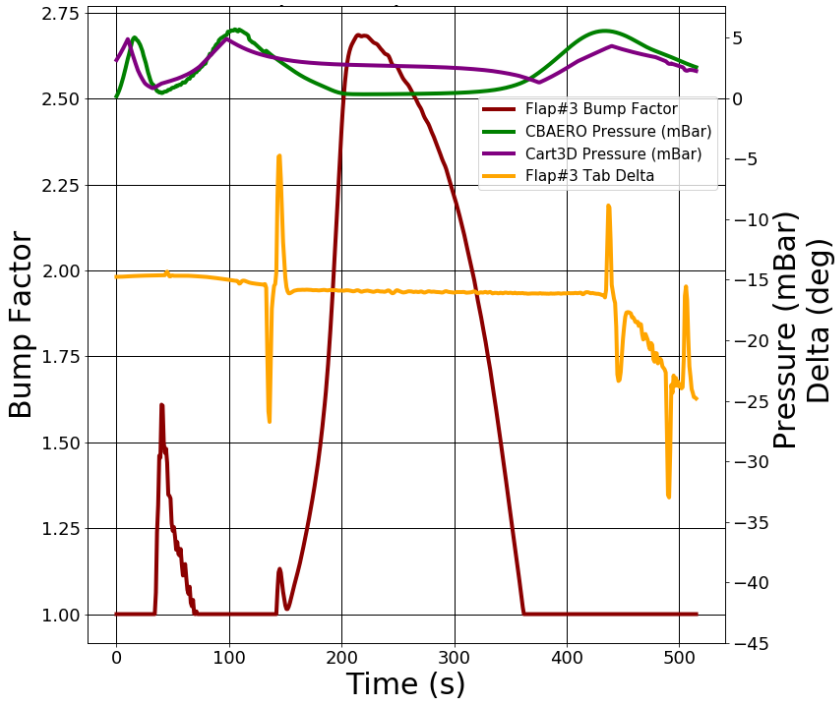

Fig. 15: Flap #3's Bump Factors, Deflection Angle, and Pressures

As Fig. 15 shows, when the Cart3D pressure (purple) is higher than the CBAERO pressure (green), the resulting bump factor is greater than one. The flat line sections are produced when the bump factor is bounded to be greater than or

equal to 1.0. Applying the bump factor to the film coefficient resulted in an increase to the overall heating. The resulting effect can be seen in the wall temperature responses for the baseline and bumped cases shown in Fig. 16.

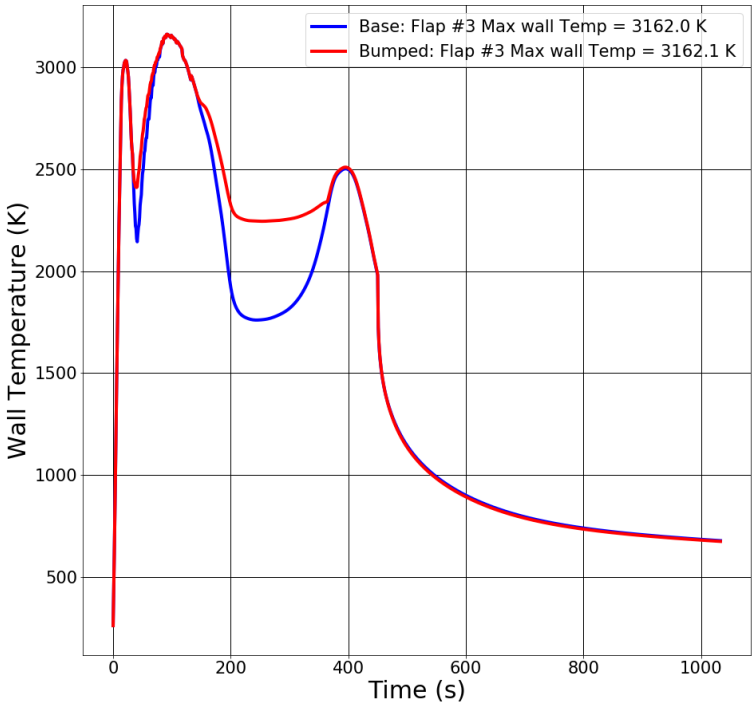

Fig. 16: Flap #3 Baseline and Bumped Wall Temperature

Additionally, the effect of the bump factor on the TPS material stack-up are illustrated in Fig. 17 which shows the TPS thicknesses for the baseline and bumped cases for the flap with the highest integrated heat load.

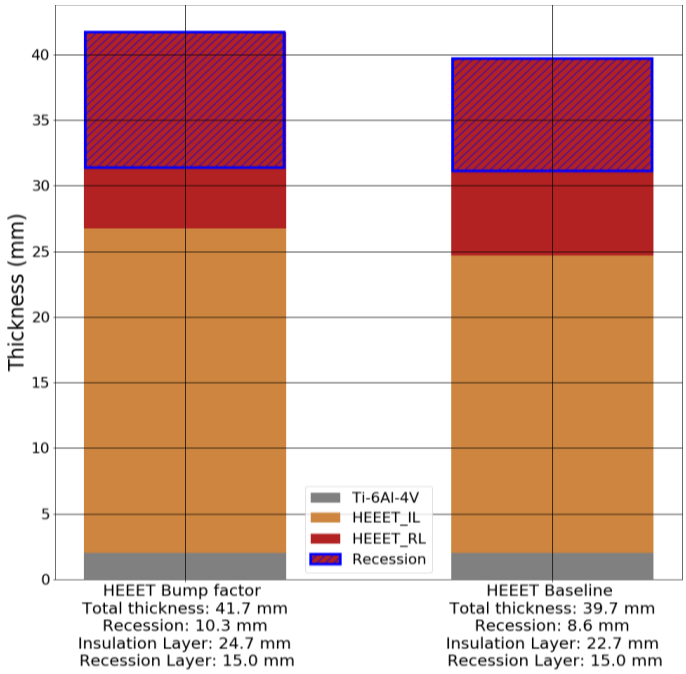

Fig. 17: Flap TPS Material Stack-up Comparison

It is worth noting that, while HEEET is ideal for high heating environments, the PBV's lifting trajectory subjects the vehicle to a high heating environment for a prolonged period of time, resulting in large amounts of predicted recession. The convective heat rate versus time for flap #3 during this trajectory is shown in Fig. 18.

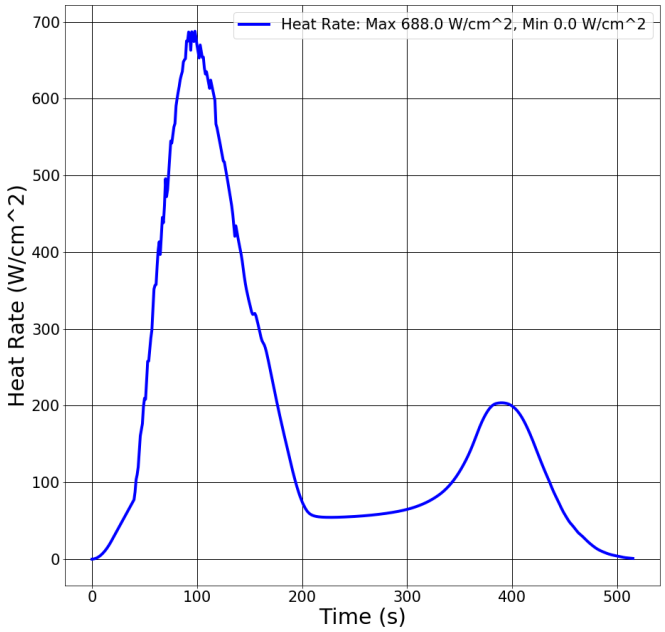

Fig. 18: Flap #3 Heat Rate vs. Time

C. Flap Results

The final flap analysis resulted in a required HEEET thickness of 41.7 mm (1.64 inches), as shown in the left stack-up in Fig. 17. The HEEET material had 10.3 mm of predicted recession and a weight per unit area of 36.6 $\frac{kg}{m^2}$ (7.5 $\frac{lb}{ft^2}$), resulting in a total flap system mass of 6.5 kg (14.3 lb).

VI. TPS Conclusions

The Pterodactyl's TPS analysis extended existing CBAERO, FIAT, and TPSSizer capabilities in order to account for flap deflection angles and sideslip angles. By including these parameters in the TPS analysis, more accurate predictions could be performed for complicated vehicles and trajectories. As interest in more complicated non-capsule entry vehicles continues to grow, the need for an TPS analysis approach that can account for more interesting entry solutions is invaluable. The analysis described in this paper discusses how the method this method was performed for the PBV's flap G&C method and nose cap while accounting for both sideslip angle and flap deflection angle variations seen during the trajectory. The Pterodactyl nose cap TPS analysis resulted in a C-PICA nose cap with a thickness of 27.0 mm and a mass of 1.22 kg. The Pterodactyl's flap control system's TPS was determined to be 41.7 mm thick HEEET with a total flap system mass of 6.5 kg.

VII. Pterodactyl Future TPS Work

The accuracy of the 1D analysis for sizing the TPS material for more complicated geometries, such as the flaps, is an area of concern. In future analysis for the Pterodactyl project, incorporating a 3D analysis at the end of the current 1D analysis to check and correct for complicated 3D geometry issues is recommended. While the current pressure ratio method to compute a bump factor allows for the addition of higher-fidelity CFD data to the sizing analysis, the anchoring could be further improved by bumping each parameter used at each discretized point on the mesh separately instead of bumping just the maximum film coefficient for each tagged region of the mesh. Lastly, looking into other potential TPS material options capable of satisfying the structural and aerothermal dynamic constraints generated by Pterodactyl mission is recommended.

Acknowledgments

The authors of this paper would like to thank NASA Space Technology Mission Directorate's Early Career Initiative (ECI) program for guiding and funding this work. Specifically, the ECI Program Executive Ricky Howard and our ECI mentor Michelle Munk. We would also like to thank our collaborators in the Engineering Systems Division, Thermal Protection Materials Branch, and Entry Systems and Vehicle Development Branch at NASA Ames Research Center: Antonella Alunni, Alan Cassell, Don Ellerby, Milad Mahzari, Frank Milos, Owen Nishioka, and Keith Peterson.

References

[1] D'Souza, S. N., Okolo, W. A., Nikaido, B. E., Yount, B. C., Tran, J., Margolis, B. W., Smith, B., Cassell, A. M., Johnson, B. J., Hibbard, K., Barton, J. D., and Hays, Z. B., "Developing an Entry Guidance and Control Design Capability Using Flaps for the Lifting Nano-ADEPT," *AIAA Aviation 2019 Forum,* AIAA, Dallas, TX, 2019.

[2] Yount, B. C., Cassell, A. M., and D'Souza, S. N., "Pterodactyl: Mechanical Designs for Integrated Control Design of a Mechanically Deployed Entry Vehicle (DEV)," *AIAA SciTech 2020 Forum,* AIAA, Orlando, FL, 2020.

[3] D'Souza, S. N., and Sarigul-Klijn, N., "Survey of Planetary Entry Guidance Algorithms," *Journal of Progress in Aerospace Sciences,* Vol. 68, 2014, pp. 64-74.

[4] TPSSizer, Software Package, Ver. 3.5a, NASA Ames Research Center, Moffett Field, CA 2019.

[5] CBAERO, Configuration Based Aerodynamics, Software Package, Ver. 5.3.3, NASA Ames Research Center, Moffett Field, CA 2019.

[6] Johnson, B. J., Rocca-Bejar, D., Lu, P., Nikaido, B. E., Yount, B. C., D'Souza, S. N., and Hays, Z. B., "Pterodactyl: Development and Performance of Guidance Algorithms for a Mechanically Deployed Entry Vehicle," *AIAA SciTech 2020 Forum,* AIAA, Orlando, FL, 2020.

[7] Nikaido, B. E., D'Souza, S. N., Hays, Z. B., and Reddish, B. J., "Pterodactyl: Aerodynamic and Aeroheating Database Development for Integrated Control Design of a Mechanically Deployed Entry Vehicle," *AIAA SciTech 2020 Forum,* AIAA, Orlando, FL, 2020.

[8] Okolo, W. A., Margolis, B. W., D'Souza, S. N., and Barton, J. D., "Pterodactyl: Development and Comparison of Control Architectures for a Mechanically Deployed Entry Vehicle," *AIAA SciTech 2020 Forum,* AIAA, Orlando, FL, 2020.

[9] FIAT, Software Package, Ver. 312, NASA Ames Research Center, Moffett Field, CA 2019.

[10] Cart3D, Software Package, Ver. 1.5.5, NASA Ames Research Center, Moffett Field, CA, 2019.

[11] Tauber, M. E., "A Review of High-Speed, Convective, Heat-Transfer Computation Methods," NASA Technical Paper 2914, No. NASA-TP-2914, 1989, pp.4-7

[12] Kinney, D. J., "Aerothermal Anchoring of CBAERO Using High Fidelity CFD," 45th AIAA Aerospace Sciences Meeting and Exhibit, 2007, pp. 4-5

[13] Tran, H. K., Johnson, C. E., Rasky, D. J., Hui, F. C. L., Hsu, M., Chen, Y. K., "Phenolic Impregnated Carbon Ablators (PICA) for Discovery Class Missions," A9636374, AIAA Paper 96-1911, June 1996.

[14] Milos, F. S., Gasch, M. J., and Prabhu, D. K., "Conformal Phenolic Impregnated Carbon Ablator (C-PICA) Arcjet Testing, Ablation and Thermal Response," 53rd AIAA Aerospace Science Meeting, Kissimmee, Florida, January 2015.

[15] Carbon-Phenolic, "Thermal Protection Materials: Thermal Physical Property Data", D. Curry, S.D. Williams, NASA Reference Publication 1289, December 1992.

[16] Milos, F. S., Chen, Y., Mahzari, M., "Arcjet Tests and Thermal Response Analysis for Dual-Layer Woven Carbon Phenolic," Journal of Spacecraft and Rockets, Vol. 55, No. 3, May-June 2018.